Delay-Dependent Stability of Single-Loop Controlled Grid-Connected Inverters with *LCL* Filters

Jianguo Wang, *Student Member, IEEE*, Jiu Dun Yan, *Member, IEEE*, Lin Jiang, *Member, IEEE*, and Jiyan Zou

***Abstract*—LCL filters have been widely used for grid-connected inverters. However, the problem that how time delay affects the stability of digitally controlled grid-connected inverters with *LCL* filters has not been fully studied. In this paper, a systematic study is carried out on the relationship between the time delay and stability of single-loop controlled grid-connected inverters that employ inverter current feedback (ICF) or grid current feedback (GCF). The ranges of time delay for system stability are analyzed and deduced in the continuous *s*-domain and discrete *z*-domain. It is shown that in the optimal range, the existence of time delay weakens the stability of the ICF loop, whereas a proper time delay is required for the GCF loop. The present work explains, for the first time, why different conclusions on the stability of ICF loop and GCF loop have been drawn in previous papers. To improve system stability, a linear predictor based time delay reduction method is proposed for ICF, while a time delay addition method is used for GCF. A controller design method is then presented that guarantees adequate stability margins. The delay-dependent stability study is verified by simulation and experiment.**

***Index Terms*—Digital control, grid-connected inverter, *LCL* filter, stability, time delay.**

I. Introduction

GRID-CONNECTED inverters form an important interface between distributed power generation systems and the power grid. *LCL* filters have been commonly adopted to mitigate switching harmonics generated by the inverters. Compared with *L* filters, *LCL* filters have better attenuating ability and allow the use of low inductance inductors, resulting in a cost-effective solution [1]. However the inherent resonance of *LCL* filters has the tendency to destabilize the inverter systems [2], [3]. Different passive and active damping methods have been proposed to improve system stability [3]-[5]. The passive damping strategy increases the power loss. The active damping methods, multi-loop or filter based, are complex in the realization and design of the controller [5]-[8].

Manuscript received September 26, 2014; revised December 18, 2014; accepted 26 January, 2015.

J. Wang, J. D. Yan and L. Jiang are with the Department of Electrical Engineering and Electronics, University of Liverpool, Liverpool, L69 3GJ, U.K., e-mail: Jianguo.Wang@liv.ac.uk; yaneee@liv.ac.uk; ljiang@liv.ac.uk.

J. Zou is with the School of Electrical Engineering, Dalian University of Technology, Dalian 116023, Liaoning, China, e-mail: jyzou@dlut.edu.cn.

Simple but effective single-loop current control methods without additional damping have been proposed and researched for the *LCL*-filtered grid-connected inverters, employing inverter current feedback (ICF) or grid current feedback (GCF) [2], [9]-[19]. It has been proved that both the ICF loop and GCF loop can be made stable because of their inherent damping characteristics [10], [14], [15].

However, the stability of the ICF and GCF loops has not been fully studied so far, especially when the time delay is taken into account. The time delay roots from the time for analog-to-digital conversion, computation, and pulse-width-modulation (PWM) generation [4], [9], [20].

Much work has been devoted to the choice of the feedback current and different conclusions on the stability of ICF loop and GCF loop have been drawn, leading to much confusion. Without considering any time delay, Tang *et al.* [10] found that the ICF loop is stable due to its inherent damping characteristics, while the GCF loop is unstable. Similar findings were also demonstrated in [11] and [12] where the grid current is indirectly controlled by the inverter current. Active damping methods are needed if the grid current is to be controlled directly [21], [22]. Considering time delay, Zhang *et al.* [9] and Bierhoff *et al.* [23] found that the ICF is still more advantageous than the GCF. Again, damping methods are necessary if the grid current is to be controlled directly [24], [25]. On the other hand, Dannehl *et al.* [2] found that GCF is superior to ICF based on stability evaluation using root loci. Similar conclusions were also drawn in [13]-[15] which showed that the GCF loop can maintain stability without any additional damping method.

Many publications have been devoted to the identification of the factors that influence the stability of the single-loop control systems. Dannehl *et al.* [2], [26] indicated that the stability is closely related to the ratio of sampling frequency to the *LCL* resonance frequency, but the nature of this relationship is not known. Yin *et al.* [15] presented the damping characteristic of the time delay in the GCF loop, and Park *et al.* [16] found that the GCF loop can be stable if the resonance frequency is smaller than $1/6$ of the sampling frequency. However only the GCF with a delay of $1.5T_s$ (T_s is the sampling period) is studied. Rui *et al.* [17] implied that the GCF loop is stable when the time delay is between $0.53T_s$ and $1.33T_s$, but this range is only valid for the controller parameters used by the authors. Zou *et al.* [18] proposed a method to obtain the stable ranges of time delay for ICF and GCF loops. However the method is not based on precise derivation, and the deduced stable ranges, which are

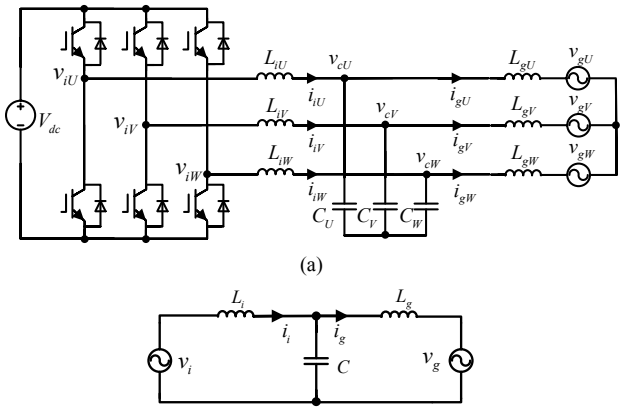

Fig. 1. A three-phase grid-connected inverter with *LCL* filters. (a) Power circuit. (b) Equivalent single-phase circuit.

different to the result in [17], are only for specified *LCL* and controller parameters.

In this paper, a thorough theoretical study is carried out on the relationship between the time delay and stability of single-loop controlled grid-connected inverters with *LCL* filters. It is found that the time delay is a key factor that affects the system stability. The main contributions of this paper are summarized below.

Firstly, the stable ranges of the time delay (the ranges of the time delay within which the system can be made stable) are deduced in the continuous *s*-domain as well as the discrete *z*-domain, applicable for any *LCL* parameters. The present study explains why different conclusions on the stability of the single-loop control systems are drawn in previous papers, i.e., the time delay in these cases falls into different ranges. Furthermore, it can be deduced that the stable ranges of time delay for the loop with capacitor current feedback are same as those of the ICF loop. Therefore the study can also facilitate the analysis of the active damping methods which employ an inner ICF or capacitor current feedback loop.

Secondly, to improve the stability of the single-loop control systems, time delay compensation methods are proposed. For ICF, a linear predictor based time delay reduction is used [27], [28]. For GCF, a proper time delay is added. By employing the proposed time delay compensators, the allowed sampling frequency ranges can be increased while still maintaining system stability.

Thirdly, a simple PI tuning method without simplification is proposed. To design the controller, the *LCL* filter is often simplified as an *L* filter [16], [19], [29]; this approach however is not accurate enough since the *LCL* resonance frequency impacts stability margins significantly. By using the proposed design method, adequate stability margins can be guaranteed.

This paper is organized as follows. Section II presents the single-loop controlled three-phase grid-connected inverter system and an analysis of the relationship between the time delay and system stability in the continuous *s*-domain. Section III provides the derivation of the stable ranges of time delay in the discrete *z*-domain. Section IV is devoted to the optimal range of the time delay and time delay compensators. A PI controller design method is proposed in Section V. Simulation and experimental results are presented in Section VI to verify the delay-dependent stability. Conclusions are finally drawn in Section VII.

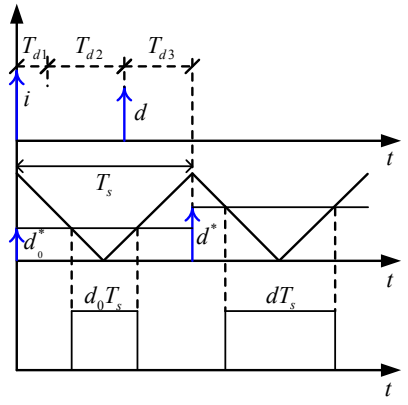

Fig. 2. Time delays in the digital control of a grid-connected inverter system.

II. Single-Loop Controlled Three-Phase Grid-Connected Inverters With *LCL* Filters

A. System Description

The circuit diagram of a three-phase grid-connected inverter with *LCL* filters is shown in Fig. 1(a), where the inverter is supplied with a constant DC voltage V_{dc}. Its equivalent single-phase circuit is shown in Fig. 1(b), where v_i is the inverter voltage and v_g the grid voltage. The inverter side inductor L_i, grid side inductor L_g, and capacitor C are the components of the *LCL* filter. The parasitic resistance associated with the inductors is neglected to represent the worst case [10], [16].

The inverter current i_i or grid current i_g can be sensed as the feedback variable for a single-loop current control system. The transfer functions from the inverter voltage to the inverter current and to the grid current are given as (1) and (2) respectively, with $\omega_r = \sqrt{1/L_gC}$ and $\omega_{res} = \sqrt{(L_i+L_g)/L_iL_gC}$.

$$G_{i_i v_i}(s) = \frac{i_i(s)}{v_i(s)} = \frac{s^2+\omega_r^2}{sL_i(s^2+\omega_{res}^2)} \tag{1}$$

$$G_{i_g v_i}(s) = \frac{i_g(s)}{v_i(s)} = \frac{\omega_r^2}{sL_i(s^2+\omega_{res}^2)} \tag{2}$$

B. Time Delay in the Control Loop

To acquire the average value of a current in a switching period and to avoid switching noises, the synchronous sampling method is commonly adopted. The currents are sampled at the beginning or the middle of a switching period [30], [31].

Taking the symmetric-on-time modulator as an example, the digital control process is shown in Fig. 2. A current is sampled when the PWM counter reaches the peak value, resulting in a sampled quantity *i*. T_{d1} represents the time for analog-to-digital conversion. With a digital controller, the duty-ratio *d* (the shadow compare register value) is calculated, and T_{d2} is the time for computation. In a digital signal processor (DSP), *d* is generally updated to the compare register (with a value of d^*, equal to *d*) when the counter reaches zero and/or the period value, leading to a duty-ratio update delay T_{d3}. The total processing delay is expressed in terms of T_s as $T_{d1}+T_{d2}+T_{d3}=$

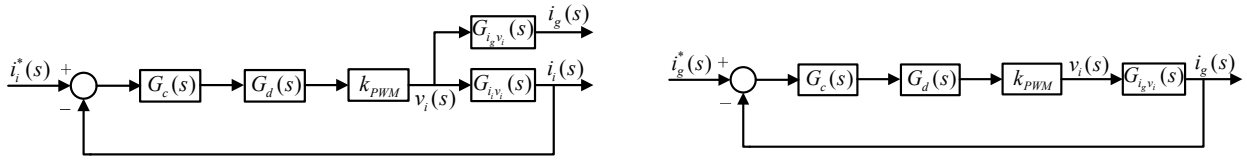

(a) (b)

Fig. 3. The *s*-domain block diagrams of the single-loop controlled grid-connected inverters. (a) ICF. (b) GCF.

λT_s. Normally, λT_s is not larger than one sampling period T_s, and its typical values in real operation are $0.5T_s$ and T_s [9], [30]. In addition to the processing delay, there is a delay T_{d4} due to the PWM, and equivalently $T_{d4} = 0.5T_s$ [27]. Therefore the total time delay in the control loop is $T_d = T_{d1} + T_{d2} + T_{d3} + T_{d4} = (\lambda + 0.5)T_s$ [20]. In the following analysis to deduce the stable ranges of time delay, λ is assumed to be a random value.

C. Analysis of the Delay-Dependent Stability in Continuous s-Domain

The block diagrams of the single-loop controlled grid-connected inverters are shown in Fig. 3. The total time delay is expressed as $G_d(s) = e^{-sT_d}$, and $k_{PWM} = V_{dc}/2$ is the gain of the PWM. $G_c(s)$ is the controller, and a PI is used:

$$G_c(s) = k_p(1+\frac{k_i}{s}). \tag{3}$$

The loop gains of the ICF and GCF are $T_i(s) = k_{PWM}G_c(s)G_d(s)G_{i_g v_i}(s)$ and $T_g(s) = k_{PWM}G_c(s)G_d(s)G_{i_g v_i}(s)$ respectively. The stability analysis is carried out using the Nyquist stability criterion. In the open-loop Bode diagram, only the frequency ranges with magnitudes above 0 dB are considered. For the phase plot in these ranges, a $\pm(2k+1)\pi$ crossing in the direction of phase rising is defined as a positive crossing, while a crossing in the direction of phase falling is defined as a negative crossing. The numbers of the positive and negative crossings are denoted as N_+ and N_- respectively [32]. According to the Nyquist stability criterion, the number of the open-loop unstable poles P must equal $2(N_+ - N_-)$ to ensure system stability, i.e., $P = 2(N_+ - N_-)$. As can be seen from (1), (2), and (3), $P = 0$, hence $N_+ - N_- = 0$ is required for both of the ICF and GCF systems.

1) Inverter Current Feedback

The magnitude (in decibels) and phase of $T_i(s)$ with $G_c(s) = k_p$ (the integral term k_pk_i/s can be designed to have a negligible influence on system stability [11]) are given in (4) and (5) respectively.

$$20\lg\left|T_i(s)\big|_{s=j\omega}\right| = 20\lg\left|k_pk_{PWM}e^{-j\omega T_d}\frac{-\omega^2+\omega_r^2}{j\omega L_i(-\omega^2+\omega_{res}^2)}\right|$$
$$= \begin{cases} 20\lg[k_pk_{PWM}\dfrac{\omega_r^2-\omega^2}{\omega L_i(\omega_{res}^2-\omega^2)}], (\omega<\omega_r) \\ -\infty, (\omega=\omega_r) \\ 20\lg[k_pk_{PWM}\dfrac{\omega^2-\omega_r^2}{\omega L_i(\omega_{res}^2-\omega^2)}], (\omega_r<\omega<\omega_{res}) \\ +\infty, (\omega=\omega_{res}) \\ 20\lg[k_pk_{PWM}\dfrac{\omega_r^2-\omega^2}{\omega L_i(\omega_{res}^2-\omega^2)}], (\omega>\omega_{res}) \end{cases} \tag{4}$$

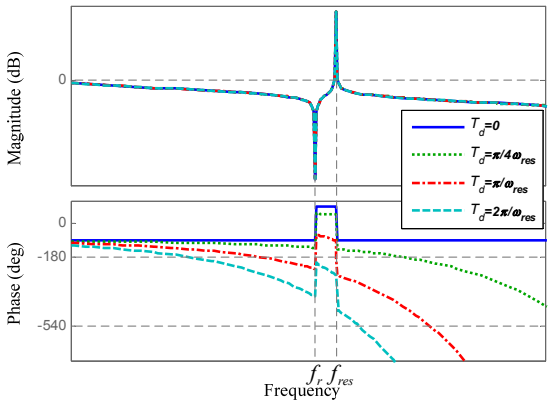

Fig. 4. Bode diagrams of the ICF loop gain with different time delays.

$$\angle T_i(s)\big|_{s=j\omega} = \angle k_pk_{PWM}e^{-j\omega T_d}\frac{-\omega^2+\omega_r^2}{j\omega L_i(-\omega^2+\omega_{res}^2)}$$
$$= \begin{cases} -\dfrac{\pi}{2}-\omega T_d, (\omega<\omega_r) \\ \dfrac{\pi}{2}-\omega T_d, (\omega_r<\omega<\omega_{res}) \\ -\dfrac{\pi}{2}-\omega T_d, (\omega>\omega_{res}) \end{cases} \tag{5}$$

The Bode diagrams of $T_i(s)$ with several different time delays are shown in Fig. 4. The magnitude at f_r ($= \omega_r/2\pi$) is definitely below 0 dB although there is a +180° jump in the phase, hence $N_+ = 0$. $N_- = 0$ is thus required for system stability. Using a sufficiently small k_p, the magnitude of $T_i(s)$ can be set below 0 dB to avoid negative crossing, except at the resonance frequency f_{res} ($= \omega_{res}/2\pi$) where the magnitude is positive infinite and there is a fall of 180° in the phase. Therefore, assuming k_p is adjustable, the system can be made stable only if the phase at f_{res} does not cross over $\pm(2k+1)\pi$. Otherwise there will be a negative crossing at f_{res} whatever k_p is, i.e., $N_- \neq 0$ and thus the system is unstable. Without any time delay, the phase at f_{res} falls from 90° to –90° and no negative crossing is generated, so the system is stable, in agreement with the findings in [10].With a finite time delay, the phase lag increases. To avoid any $\pm(2k+1)\pi$ crossing at f_{res}, it can be derived from (5) that the time delay should fall into one of the following ranges:

$$\begin{cases} T_d < \dfrac{\pi}{2\omega_{res}}, (k=0) \\ \dfrac{(4k-1)\pi}{2\omega_{res}} < T_d < \dfrac{(4k+1)\pi}{2\omega_{res}}, (k=1,2,3...) \end{cases} \tag{6}$$

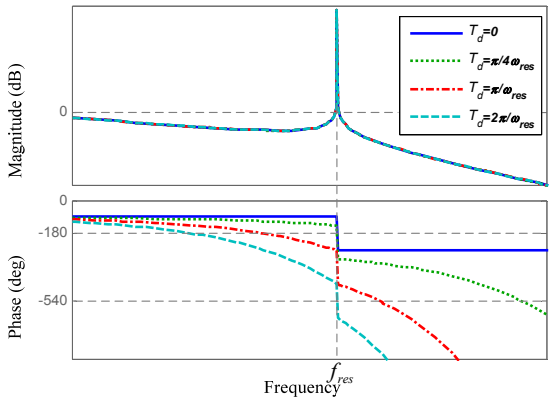

Fig. 5. Bode diagrams of the GCF loop gain with different time delays.

2) Grid Current Feedback

The magnitude (in decibels) and phase of $T_g(s)$ with $G_c(s) = k_p$ are given as (7) and (8) respectively.

$$20\lg\left|T_g(s)\right|_{s=j\omega}\Big| = 20\lg\left|k_p k_{PWM} e^{-j\omega T_d}\frac{\omega_r^2}{j\omega L_i(-\omega^2+\omega_{res}^2)}\right|$$
$$= \begin{cases} 20\lg[k_p k_{PWM}\dfrac{\omega_r^2}{\omega L_i(\omega_{res}^2-\omega^2)}], (\omega<\omega_{res}) \\ +\infty, (\omega=\omega_{res}) \\ 20\lg[k_p k_{PWM}\dfrac{\omega_r^2}{\omega L_i(\omega^2-\omega_{res}^2)}], (\omega>\omega_{res}) \end{cases} \quad (7)$$

$$\angle T_g(s)\Big|_{s=j\omega} = \angle k_p k_{PWM} e^{-j\omega T_d}\frac{\omega_r^2}{j\omega L_i(-\omega^2+\omega_{res}^2)}$$
$$= \begin{cases} -\dfrac{\pi}{2}-\omega T_d, (\omega<\omega_{res}) \\ -\dfrac{3\pi}{2}-\omega T_d, (\omega>\omega_{res}) \end{cases} \quad (8)$$

The Bode diagrams of $T_g(s)$ with different time delays are shown in Fig. 5. Similar to the ICF loop, the GCF loop can be made stable if there is no negative crossing at f_{res}, i.e., the phase at f_{res} does not cross over $\pm(2k+1)\pi$. Without any time delay, the phase at f_{res} falls from –90° to –270° and a negative crossing exists, the system is thus unstable. To avoid any potential negative crossing at f_{res}, it can be deduced from (8) that the time delay should be in the following ranges:

$$\frac{(4k+1)\pi}{2\omega_{res}} < T_d < \frac{(4k+3)\pi}{2\omega_{res}}, (k=0,1,2,\ldots), \quad (9)$$

which indicates that a proper time delay is necessary for the stability of GCF loop.

III. Analysis of the Delay-Dependent Stability in Discrete z-Domain

In this section, the delay-dependent stability of the single-loop controlled grid-connected inverters with *LCL* filters is studied in the discrete *z*-domain. The proportional gain k_p is assumed to be adjustable. Then the stable ranges of the time delay for ICF and GCF loops are deduced, based on the requirement that when the time delay is in the stable ranges all discrete closed-loop poles should be inside the unit circle if an infinitely small k_p is used. On the other hand, if the time delay is outside the stable ranges, there will be unstable closed-loop poles outside the unit circle whatever k_p is.

A. Discrete Models

To obtain the discrete models, the processing delay and PWM are analyzed separately. The processing delay is expressed as $e^{-s\lambda T_s}$. The PWM is usually modeled as a zero-order-hold (ZOH) [33], that is

$$G_{PWM}(s) = \frac{1-e^{-sT_s}}{s}. \quad (10)$$

A more precise PWM model has been proposed in [9] and [30] and is expressed as

$$G'_{PWM}(s) = \frac{T_s}{2}(e^{-s\frac{T_s}{4}} + e^{-s\frac{3T_s}{4}}). \quad (11)$$

The frequency domain models of (10) and (11) are denoted as

$$G_{PWM}(j\omega) = \frac{1-e^{-j\omega T_s}}{j\omega} = \frac{\sin\dfrac{\omega T_s}{4}\cos\dfrac{\omega T_s}{4}}{\dfrac{\omega}{4}}e^{-j\omega\frac{T_s}{2}} \quad (12)$$

and

$$G'_{PWM}(j\omega) = \frac{T_s}{2}(e^{-j\omega\frac{T_s}{4}} + e^{-j\omega\frac{3T_s}{4}}) = T_s\cos\frac{\omega T_s}{4}e^{-j\omega\frac{T_s}{2}} \quad (13)$$

respectively. It can be seen that the time delays of these two PWM models are identical ($0.5T_s$), and their magnitude gains are almost same because a small T_s is commonly used. Therefore the ZOH model (10) is adequate for the discrete analysis [33].

The block diagrams of the single-loop digitally controlled grid-connected inverters are shown in Fig. 6, where $G_{PWM}(s)$ is given in (10), and $G_c(z)$ is the discrete equivalent of $G_c(s)$ [30]. To obtain the closed-loop discrete transfer functions of the two control systems, the discrete transfer function from $d(z)$ to $i_i(z)$ and $i_g(z)$ should be obtained first. Therefore *z*-transform is used to obtain the discrete transfer functions of the paths which contain the processing delay, PWM, and the plant transfer functions $G_{i_i v_i}(s)$ and $G_{i_g v_i}(s)$ followed by ideal samplers. For a plant transfer function $G(s)$, the discrete transfer function is expressed as [9], [30]

$$G(z) = Z\{e^{-s\lambda T_s}G_{PWM}(s)k_{PWM}G(s)\}$$
$$= k_{PWM}\frac{z-1}{z^{\ell+1}}Z\{\frac{G(s)}{s}e^{smT_s}\}, \quad (14)$$

where ℓ is an integer, $0 \le m < 1$, and $\lambda = \ell - m$. $Z\{\dfrac{G(s)}{s}e^{smT_s}\}$ in (14) can be obtained using the following property [33]:

$$Z\{\frac{G(s)}{s}e^{smT_s}\} = \sum_{i=1}^{n}\mathrm{Res}[\frac{zG(s)e^{smT_s}}{s(z-e^{sT_s})}]_{s=p_i}, \quad (15)$$

where p_i ($i = 1, 2, \ldots, n$) are the poles of $G(s)/s$ and Res denotes the residue.

Substituting $G_{i_i v_i}(s)$ and $G_{i_g v_i}(s)$ for $G(s)$ in (14) and (15), the discrete transfer functions from $d(z)$ to $i_i(z)$ and $i_g(z)$ are obtained as (16) and (17) respectively.

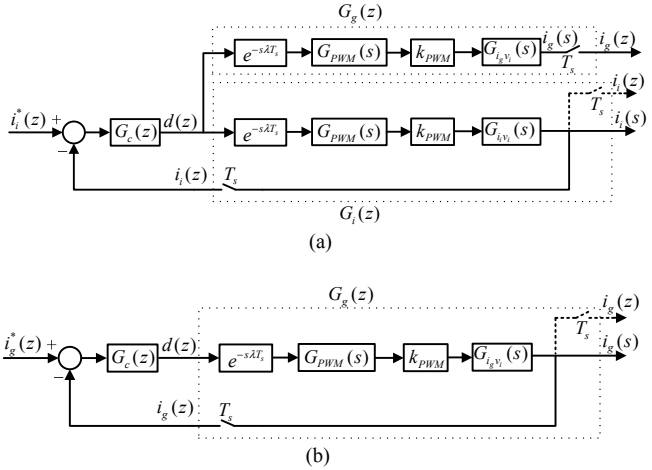

Fig. 6. Block diagrams of the single-loop digitally controlled grid-connected inverters. (a) ICF. (b) GCF.

$$G_i(z) = k_{PWM}\frac{z-1}{z^{\ell}}\Big[\frac{T_s}{L_i+L_g}\frac{mz+1-m}{(z-1)^2} + \frac{L_g}{L_i(L_i+L_g)\omega_{res}}\frac{z\sin m\omega_{res}T_s+\sin(1-m)\omega_{res}T_s}{z^2-2z\cos\omega_{res}T_s+1}\Big] \tag{16}$$

$$G_g(z) = k_{PWM}\frac{z-1}{z^{\ell}}\Big[\frac{T_s}{L_i+L_g}\frac{mz+1-m}{(z-1)^2} - \frac{1}{(L_i+L_g)\omega_{res}}\frac{z\sin m\omega_{res}T_s+\sin(1-m)\omega_{res}T_s}{z^2-2z\cos\omega_{res}T_s+1}\Big] \tag{17}$$

Therefore, the closed-loop transfer functions of the control loops with ICF and GCF are given as (18) and (19) respectively.

$$G_{icl}(z) = \frac{i_g(z)}{i_i^*(z)} = \frac{G_c(z)G_g(z)}{1+G_c(z)G_i(z)} \tag{18}$$

$$G_{gcl}(z) = \frac{i_g(z)}{i_g^*(z)} = \frac{G_c(z)G_g(z)}{1+G_c(z)G_g(z)} \tag{19}$$

A discrete closed-loop is stable if all the poles are inside the unit circle. From (16) and (17) it can be seen that the ICF and GCF have the same open-loop poles, and three are on the unit circle ($z_1 = 1$, $z_{2,3} = \cos\omega_{res}T_s \pm j\sin\omega_{res}T_s$). Thus with $G_c(z) = k_p$, for a possible stable operation, i.e. the time delay being in the stable ranges, all the closed-loop poles should be inside the unit circle when an infinitely small k_p is used. On the other hand, if the time delay is outside the stable ranges, there will be unstable closed-loop poles outside the unit circle whatever k_p is.

The w-transform $z = (w + 1)/(w - 1)$ is used to map the area inside the unit circle in the z-plane into the left half-plane (LHP) of the w-plane, such that the Routh's stability criterion can be used [32]. The stable ranges of the time delay can be derived based on the requirement that the roots of $D_i(w) = 1 + k_pG_i(w) = 0$ and $D_g(w) = 1 + k_pG_g(w) = 0$ should be in the LHP when an infinitely small k_p is used. An exemplary derivation for GCF with the case of $0 < \lambda \le 1$, i.e., $\ell = 1$ and $0 \le m < 1$, is provided in the Appendix. The stable ranges of GCF with other cases of λ can also be derived using the same method, as well as those of the ICF.

B. Inverter Current Feedback

Using the method in the Appendix, the general requirement for the stability of the ICF loop can be obtained as

$$\begin{aligned}&\sin[(\ell+1-m)\omega_{res}T_s] > \sin[(\ell-m)\omega_{res}T_s]\\ &\Rightarrow \sin[(\lambda+1)\omega_{res}T_s] > \sin(\lambda\omega_{res}T_s),\end{aligned} \tag{20}$$

which results in $(\lambda+\frac{1}{2})T_s < \frac{\pi}{2\omega_{res}}$ $(k=0)$, $\frac{(4k-1)\pi}{2\omega_{res}} < (\lambda+\frac{1}{2})T_s < \frac{(4k+1)\pi}{2\omega_{res}}$ $(k=1,2,3...)$, the same as (6) that was deduced in the s-domain. However for controllability, f_{res} should be smaller than half the sampling frequency ($f_s/2$, the Nyquist frequency), i.e., $\omega_{res}T_s < \pi$ [32], [34]. Considering this restriction, the stable ranges of the time delay are obtained as (21), shown at the bottom of this page.

It is interesting from (21) that for a given T_s, the system can be stabilized by modifying the value of λ, and vice versa. Moreover, there are many optional ranges for λ and T_s. Taking $\lambda = 3$ for example, the available values of k are 0 and 1; therefore the resultant condition is $T_s \in (0, \pi/7\omega_{res}) \cup (3\pi/7\omega_{res}, 5\pi/7\omega_{res})$. The root loci of the closed-loop system with T_s in different ranges are shown in Fig. 7, which demonstrate that there are at least two unstable poles outsider the unit circle if the condition is not met.

C. Grid Current Feedback

Using the method in the Appendix, the following stable condition can be obtained for the GCF loop:

$$\begin{aligned}&\sin[(\ell+1-m)\omega_{res}T_s] < \sin[(\ell-m)\omega_{res}T_s]\\ &\Rightarrow \sin[(\lambda+1)\omega_{res}T_s] < \sin(\lambda\omega_{res}T_s),\end{aligned} \tag{22}$$

$$\begin{cases}(\lambda+\frac{1}{2})T_s < \frac{\pi}{2\omega_{res}}, (\lambda \ge k, k=0)\\ \frac{(4k-1)\pi}{2\omega_{res}} < (\lambda+\frac{1}{2})T_s < (\lambda+\frac{1}{2})\frac{\pi}{\omega_{res}}, (2k-1 < \lambda \le 2k, k=1,2,3,...)\\ \frac{(4k-1)\pi}{2\omega_{res}} < (\lambda+\frac{1}{2})T_s < \frac{(4k+1)\pi}{2\omega_{res}}, (\lambda > 2k, k=1,2,3,...)\end{cases} \tag{21}$$

$$\begin{cases}\frac{(4k+1)\pi}{2\omega_{res}} < (\lambda+\frac{1}{2})T_s < (\lambda+\frac{1}{2})\frac{\pi}{\omega_{res}}, (2k < \lambda \le 2k+1, k=0,1,2,...)\\ \frac{(4k+1)\pi}{2\omega_{res}} < (\lambda+\frac{1}{2})T_s < \frac{(4k+3)\pi}{2\omega_{res}}, (\lambda > 2k+1, k=0,1,2,...)\end{cases} \tag{23}$$

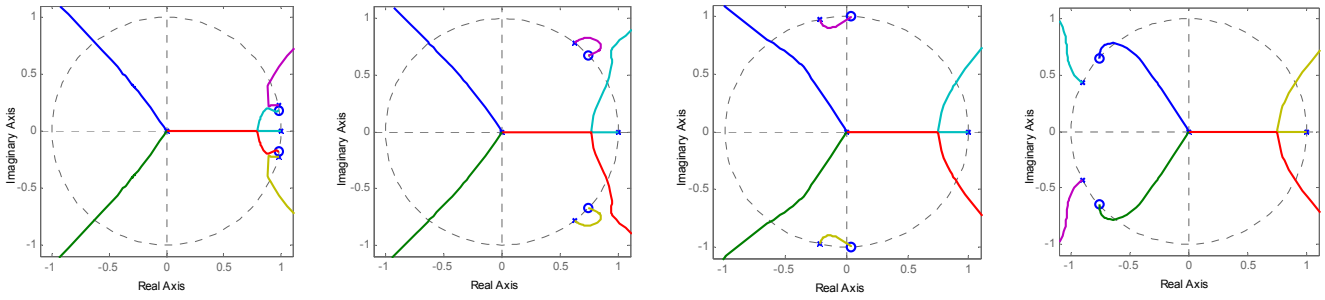

Fig. 7. Root loci of the ICF loop when $\lambda = 3$ and with T_s in different ranges. (a) $T_s \in (0, \pi/7\omega_{res})$. (b) $T_s \in (\pi/7\omega_{res}, 3\pi/7\omega_{res})$. (c) $T_s \in (3\pi/7\omega_{res}, 5\pi/7\omega_{res})$. (d) $T_s \in (5\pi/7\omega_{res}, \pi/\omega_{res})$.

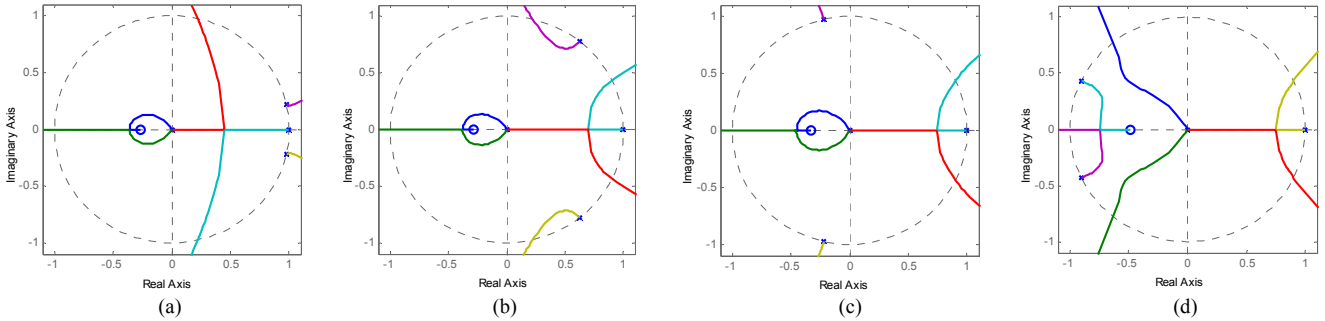

Fig. 8. Root loci of the GCF loop when $\lambda = 3$ and with T_s in different ranges. (a) $T_s \in (0, \pi/7\omega_{res})$. (b) $T_s \in (\pi/7\omega_{res}, 3\pi/7\omega_{res})$. (c) $T_s \in (3\pi/7\omega_{res}, 5\pi/7\omega_{res})$. (d) $T_s \in (5\pi/7\omega_{res}, \pi/\omega_{res})$.

which results in $\frac{(4k+1)\pi}{2\omega_{res}} < (\lambda+\frac{1}{2})T_s < \frac{(4k+3)\pi}{2\omega_{res}}$ $(k = 0,1,2,...)$, the same as (9) that was derived in the *s*-domain. Also considering the restriction $\omega_{res}T_s < \pi$, the stable ranges of the time delay are yielded as (23), shown at the bottom of the former page.

Like ICF, the GCF loop can also be stabilized by adjusting the value of λ or T_s. For example, for the case of $\lambda = 3$, the available values of k are 0 and 1, thus the stable ranges of T_s are $(\pi/7\omega_{res}, 3\pi/7\omega_{res}) \cup (5\pi/7\omega_{res}, \pi/\omega_{res})$. The root loci of the closed-loop system with T_s in different ranges are shown in Fig. 8. As seen if T_s is outside the stable ranges, there are at least two unstable poles whatever the proportional gain k_p is.

It can be seen from (6) and (9), (21) and (23) that the stable ranges of the time delay for ICF and GCF are complementary. It means that with a given time delay, only one of them can be made stable if no time delay compensator is applied.

IV. Optimal Range of Time Delay and Compensators

In this section the optimal range of the time delay is discussed and identified, to achieve the maximum bandwidth and ensure adequate stability margins. It is found that in the optimal range, the existence of time delay degrades the stability of the ICF loop, whereas a proper time delay is needed for the GCF loop. To improve stability, a linear predictor based time delay reduction method is proposed for ICF, while a proper time delay can be added for GCF.

A. Reasonable Time Delay Range

The stable ranges (21) and (23) indicate that there are many available ranges for the time delay. However, for a large k, the phase lag due to the time delay is significant. Small controller gains have to be used to guarantee stability, leading to a low bandwidth. From (21) and (23), it can be seen that $k = 0$ is the case for achieving the highest bandwidth. The reasonable time delay ranges of ICF and GCF are thus given as (24) and (25) respectively.

TABLE I
Stable and Optimal Ranges of the Sampling Frequency

method	λ	stable range	optimal range
ICF	0.5	$f_s > 4f_{res}$	$f_s > 6f_{res}$
	1	$f_s > 6f_{res}$	$f_s > 9f_{res}$
GCF	0.5	$2f_{res} < f_s < 4f_{res}$	$2f_{res} < f_s < 3f_{res}$
	1	$2f_{res} < f_s < 6f_{res}$	$9f_{res}/4 < f_s < 9f_{res}/2$

$$(\lambda+\frac{1}{2})T_s < \frac{\pi}{2\omega_{res}}, (\lambda \geq 0) \tag{24}$$

$$\begin{cases} \frac{\pi}{2\omega_{res}} < (\lambda+\frac{1}{2})T_s < (\lambda+\frac{1}{2})\frac{\pi}{\omega_{res}}, (0 < \lambda \leq 1) \\ \frac{\pi}{2\omega_{res}} < (\lambda+\frac{1}{2})T_s < \frac{3\pi}{2\omega_{res}}, (\lambda > 1) \end{cases} \tag{25}$$

From (24) it can be seen that an increase in time delay degrades the stability of the ICF loop. However for the GCF, (25) indicates that a proper time delay is required for the stability of the GCF loop, and that in the scale of $0 < \lambda \leq 1$, $\lambda = 1$ is the best option to get the largest available range of the sampling period T_s.

For a given λ, requirements (24) and (25) can also be used to calculate the stable range of f_s. Taking $\lambda = 0.5$ and $\lambda = 1$ for example, the ranges of f_s are given in Table I. Note that the requirement of GCF for $\lambda = 1$ is in agreement with the findings in [16].

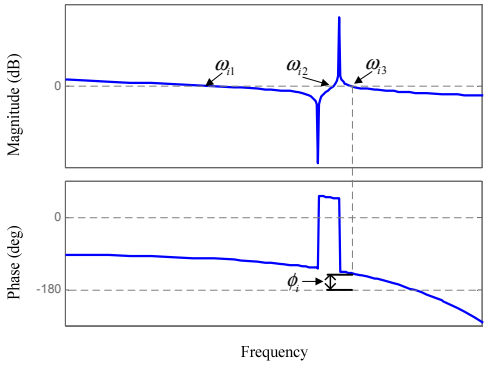

Fig. 9. Bode diagram of the ICF loop gain with time delay in the optimal range.

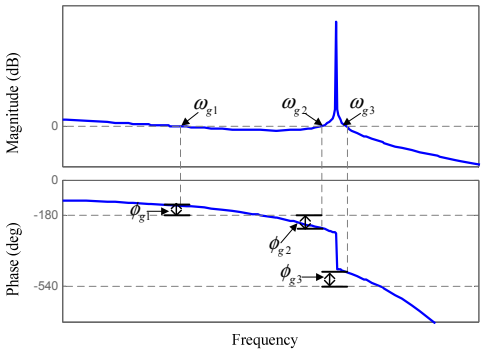

Fig. 10. Bode diagram of the GCF loop gain with time delay in the optimal range.

B. Optimal Time Delay Range

A system can be made stable when the time delay falls into the stable ranges. However, the possible stable operation is not enough, adequate stability margins including phase margin (PM) and gain margin (GM) should also be considered.

For the ICF, when the time delay is within the stable range (24), the Bode diagram of the loop gain is shown in Fig. 9. There are three crossover frequencies: ω_{i1}, ω_{i2}, and ω_{i3} ($\omega_{i1} < \omega_r$, $\omega_r < \omega_{i2} < \omega_{res}$, $\omega_{i3} > \omega_{res}$). It is apparent that the PM of ϕ_i at ω_{i3} is the smallest one. For a predetermined PM of φ ($\varphi < \pi/2$), to ensure a possibility for $\phi_i \geq \varphi$, the phase lag of the time delay at ω_{res} should be smaller than $\pi/2 - \varphi$, that is

$$(\lambda + \frac{1}{2})T_s < \frac{\pi/2 - \varphi}{\omega_{res}}. \tag{26}$$

For the GCF, based on (25), the Bode diagram of the loop gain is shown in Fig. 10. There are also three crossover frequencies: ω_{g1}, ω_{g2}, and ω_{g3}. ϕ_{g1} can be modified to be larger than φ by adjusting k_p. To make it possible for $\phi_{g2} \geq \varphi$ and $\phi_{g3} \geq \varphi$, the following optimal range of the time delay can be obtained:

$$\begin{cases} \dfrac{\pi/2+\varphi}{\omega_{res}} < (\lambda+\dfrac{1}{2})T_s < (\lambda+\dfrac{1}{2})\dfrac{\pi}{\omega_{res}}, (\dfrac{\varphi}{\pi} < \lambda \leq 1 - \dfrac{\varphi}{\pi}) \\ \dfrac{\pi/2+\varphi}{\omega_{res}} < (\lambda+\dfrac{1}{2})T_s < \dfrac{3\pi/2-\varphi}{\omega_{res}}, (\lambda > 1 - \dfrac{\varphi}{\pi}) \end{cases} \tag{27}$$

To sum up, to make it is possible for PM to be larger than φ, the time delay of the ICF and GCF must fall into the optimal range (26) and (27) respectively. For a given λ, the optimal range of f_s can also be deduced. Taking $\varphi = \pi/6$ (30°) for instance, the optimal range of f_s for $\lambda = 0.5$ and $\lambda = 1$ are also summarized in Table I.

C. Time Delay Compensators

1) Time Delay Reduction for ICF

As stated previously, the time delay weakens the stability of the ICF loop. Therefore, time delay reduction methods should be adopted if (26) is not met. Numerous compensators have been proposed, such as the state observers [24] and shifting of sampling constants [32], [33]. However, the state observers are sensitive to the parameter variations, and the shifting of the sampling constants is limited by aliasing and switching noises [32]. A linear predictor (LP) as described in [27] is adopted in the present work due to its effectiveness and ease of realization. Its discrete transfer function is given as

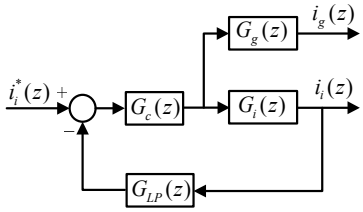

Fig. 11. Block diagram of the ICF loop with a linear predictor.

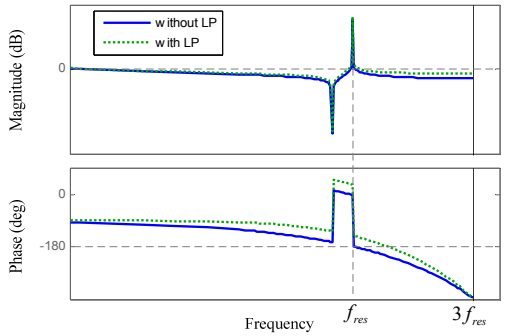

Fig. 12. Bode diagrams of the loop gain of ICF when $\lambda = 1$ and $f_s = 6f_{res}$, with and without the linear predictor.

$$G_{LP}(z) = 1 + \frac{T_d}{T_s} - \frac{T_d}{T_s} z^{-1} = \lambda + \frac{3}{2} - (\lambda + \frac{1}{2}) z^{-1}. \tag{28}$$

The compensated block diagram is shown in Fig. 11, where the LP is in the feedback loop [20]. Taking $\lambda = 1$ for example, Table I indicates that $f_s = 6f_{res}$ is the critical sampling frequency. However, with the adoption of the linear predictor, the phase margin is increased significantly as shown in Fig. 12, thus the stability is improved.

Using the previous procedure, it can be deduced that the stable ranges of time delay for the loop with capacitor current feedback, which is usually adopted as an inner active damping loop [26], are the same as those of the ICF loop. This is why time delay reduction methods are employed to eliminate the non-minimum phase behavior of the inner loop, thus to improve the overall system stability [25], [32]. Therefore, the present work can also facilitate the analysis of the active damping methods with an inner loop using the capacitor current feedback or ICF [3].

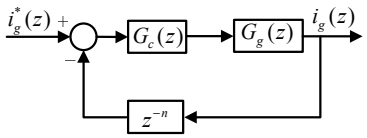

Fig. 13. Block diagram of the GCF loop with an addition of time delay.

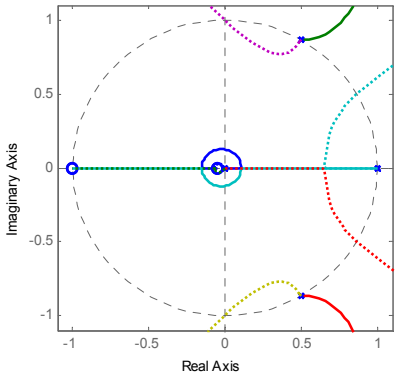

Fig. 14. Root loci of the GCF loop when $f_s = 6f_{res}$, with $\lambda = 0.5$ (solid lines) and $\lambda = 2.5$ (dotted lines).

2) A Proper Time Delay Added for GCF

For a given $f_s > 2f_{res}$, if (27) is not fulfilled, λ should generally be increased properly. The available range of λ can be yielded as

$$(\frac{1}{4}+\frac{\varphi}{2\pi})\frac{f_s}{f_{res}}-\frac{1}{2}<\lambda<(\frac{3}{4}-\frac{\varphi}{2\pi})\frac{f_s}{f_{res}}-\frac{1}{2}. \quad (29)$$

The corresponding compensated block diagram is shown in Fig. 13, where a delay z^{-n} is added so that the processing time delay fulfills (29). In the real operation, λ is an integer multiple of 0.5 [9], this should be considered when using (29).

Taking $\lambda = 0.5$, $f_s = 6f_{res}$ for example, Table I and the root loci in Fig. 14 indicate an unstable system. According to (29), the optimal range for $\varphi = 30°$ is $1.5 < \lambda < 3.5$. The root loci of the system with a compromise value $\lambda = 2.5$ ($n = 2$) are shown in Fig. 14. It can be seen that the system can be stabilized by adding a proper time delay.

D. Discussion on the Choice of the Feedback Current

Confusions exist in conclusions and findings relevant to the stability of the single-loop control systems from different previous work. The analysis in the present work is able to clarify the confusions and provide a unified explanation.

Without considering any time delay, the ICF loop can be made stable while the GCF loop can never be stabilized without other measures. This is why the inverter current was chosen as the control variable in [10]-[12], [35]. The GCF has only been used with additional active damping methods [3], [6], [7], [22].

In previous papers, the total time delay is predominantly considered to be $T_d = 1.5T_s$ ($\lambda = 1$). In this case, as indicated in Table I, the ICF loop can be made stable when $f_s > 6f_{res}$, while the requirement for GCF is $2f_{res} < f_s < 6f_{res}$. In [9], $f_{res} = 1756.5$ Hz and $f_s = 20000$ Hz gives $f_s/f_{res} = 11.3863$, then it was found the ICF is superior to the GCF. Similar results were also given in [23] ($f_{res} = 726.44$ Hz and $f_s = 5000$ Hz, $f_s/f_{res} = 6.8829$) and [24] ($f_{res} = 1136.8$ Hz and $f_s = 10000$Hz, $f_s/f_{res} = 8.7966$), which showed that the active damping is required if the grid current is to be controlled directly [25].

On the other hand, in [2], $f_{res} = 1224.1$ Hz and $f_s \in$ (3500 Hz, 7000 Hz) thus $f_s/f_{res} \in$ (2.8592, 5.7185), then it concluded that the GCF loop is stable whereas the ICF loop is unstable. Similar conclusions were also drawn in [14] ($f_{res} = 2219.3$ Hz and $f_s = 8000$ Hz, $f_s/f_{res} = 3.6047$) and [15] ($f_{res} \in$ (2905.8 Hz, 5058.3 Hz) and $f_s = 16000$ Hz, $f_s/f_{res} \in$ (3.1631, 5.5062)) by using the grid current as the feedback variable.

From aforementioned analyses, the choice of the feedback current should be made based on the *LCL* parameters. For a low *LCL* resonance frequency, it is better to choose the inverter current to obtain a large stable range of the sampling frequency. For a high *LCL* resonance frequency, the grid current can be used to avoid a too high sampling frequency. In some cases, both of these two currents can be adopted with the proposed time delay compensators applied.

Finally, the robustness of the single-loop control systems against the grid inductance variation is discussed. The addition of a grid inductance is equivalent to an increase in L_g, hence leading to a lower ω_{res} ($\omega_{res} = \sqrt{(L_i + L_g)/L_i L_g C}$). For the ICF, it can be seen from (24) and (26) that the available time delay range is increased. The ICF is therefore robust to the grid inductance variation. For the GCF, (25) and (27) indicate that the decreased ω_{res} shifts the available time delay range. The previous time delay in the system would not be covered by the shifted stable range. Therefore, the GCF is susceptible to the grid inductance variation.

V. Design of the Controller

Now that a single-loop control system can be stabilized if the time delay is in the stable ranges, and the optimal range makes it is possible for the PM to be larger than a predetermined value, the PI controller has to be designed to guarantee adequate stability margins.

The design of PI controller for an *LCL*-filtered inverter is usually implemented by simplifying the *LCL* as an *L* filter [6], [16], [19]. However from previous analysis, the *LCL* resonance affects the stability margins significantly, this approximation is thus not accurate enough. In this section, a simple tuning procedure is proposed. This method is also suitable for the proportional resonant (PR) controller.

A. Inverter Current Feedback

Firstly, the proportional gain k_p is discussed. There are three main values, k_{p1} to achieve a PM of φ, k_{p2} to ensure a GM of 3 dB [35], and the maximum value $k_{p\max}$ to ensure stability.

For a predetermined PM of φ, according to (5) the crossover frequency ω_{i3} in Fig. 9 can be yielded as

$$\varphi = \pi - \frac{\pi}{2} - (\lambda + \frac{1}{2})\omega_{i3}T_s \Rightarrow \omega_{i3} = \frac{\pi - 2\varphi}{(2\lambda+1)T_s}. \quad (30)$$

k_{p1} is then set to achieve unity loop gain at ω_{i3}, according to (4) the following is obtained

$$k_{p1} = \frac{\omega_{i3}L_i(\omega_{i3}^2 - \omega_{res}^2)}{k_{PWM}(\omega_{i3}^2 - \omega_r^2)}. \quad (31)$$

The frequency ω_m at which the phase of the open-loop transfer function crosses over –180° is given as

$$(\lambda+\frac{1}{2})\omega_m T_s=\frac{\pi}{2}\Rightarrow\omega_m=\frac{\omega_s}{2(2\lambda+1)}, \tag{32}$$

where $\omega_s=2\pi f_s$. $k_{p\max}$ is then set to achieve unity at ω_m, given as

$$k_{p\max}=\frac{\omega_s L_i[\omega_s^2-4(2\lambda+1)^2\omega_{res}^2]}{k_{PWM}[2(2\lambda+1)\omega_s^2-8(2\lambda+1)^3\omega_r^2]}. \tag{33}$$

k_{p2} to ensure a GM of 3 dB is therefore expressed as

$$k_{p2}=\frac{\sqrt{2}}{2}\frac{\omega_s L_i[\omega_s^2-4(2\lambda+1)^2\omega_{res}^2]}{k_{PWM}[2(2\lambda+1)\omega_s^2-8(2\lambda+1)^3\omega_r^2]}. \tag{34}$$

As a result, k_p is chosen to be the smaller one of k_{p1} and k_{p2}.

Finally the integral gain k_i can be tuned to make a small phase contribution at $\omega_{res}/2$, given as [10], [29]

$$k_i=\frac{\omega_{res}}{20}. \tag{35}$$

If a LP (28) is applied to enhance the stability, the parameters should be modified. The magnitude and phase of the loop gain becomes $|T_i(z)|=|k_{PWM}G_c(z)G_{LP}(z)G_i(z)|$ and $\angle T_i(z)=\angle k_{PWM}G_c(z)G_{LP}(z)G_i(z)$ respectively. The magnitude and phase of the LP are

$$\begin{cases}\left|G_{LP}(\omega)\right|=\dfrac{\sqrt{8\lambda^2+16\lambda+10-(8\lambda^2+16\lambda+6)\cos\omega T_s}}{2},\\ \theta_{LP}(\omega)=\arctan\dfrac{(2\lambda+3)\sin\omega T_s}{(2\lambda+3)\cos\omega T_s-(2\lambda+1)}-\omega T_s+\pi.\end{cases} \tag{36}$$

Therefore following the same tuning procedure above, k_{p1} and k_{p2} can be calculated as

$$\begin{cases}k_{p1}=\dfrac{\omega_{i3}L_i(\omega_{i3}^2-\omega_{res}^2)}{k_{PWM}(\omega_{i3}^2-\omega_r^2)\left|G_{LP}(\omega_{i3})\right|}\\ k_{p2}=\dfrac{\sqrt{2}}{2}\dfrac{\omega_m L_i(\omega_m^2-\omega_{res}^2)}{k_{PWM}(\omega_m^2-\omega_r^2)\left|G_{LP}(\omega_{i3})\right|},\end{cases} \tag{37}$$

where ω_{i3} and ω_m are modified as

$$\omega_{i3}=\frac{\pi-2\varphi+2\theta_{LP}(\omega_{i3})}{(2\lambda+1)T_s},\omega_m=\frac{\pi+2\theta_{LP}(\omega_m)}{(2\lambda+1)T_s}. \tag{38}$$

The integral gain k_i is still given by (35).

B. Grid Current Feedback

On the basis of (27), to achieve a PM of φ, the crossover frequencies ω_{g1}, ω_{g2}, and ω_{g3} are obtained from (8) as

$$\omega_{g1}=\frac{\pi-2\varphi}{(2\lambda+1)T_s},\omega_{g2}=\frac{\pi+2\varphi}{(2\lambda+1)T_s},\omega_{g3}=\frac{3\pi-2\varphi}{(2\lambda+1)T_s}. \tag{39}$$

The corresponding proportional gains are then derived from (7) as

$$\begin{cases}k_{p1}=\dfrac{\omega_{g1}L_i(\omega_{res}^2-\omega_{g1}^2)}{k_{PWM}\omega_r^2},\\ k_{p2}=\dfrac{\omega_{g2}L_i(\omega_{res}^2-\omega_{g2}^2)}{k_{PWM}\omega_r^2},\\ k_{p3}=\dfrac{\omega_{g3}L_i(\omega_{g3}^2-\omega_{res}^2)}{k_{PWM}\omega_r^2}.\end{cases} \tag{40}$$

The frequency ω_m at which the phase of the open-loop transfer function crosses over –180° is the same as (32). The maximum value $k_{p\max}$, and k_{p4} to give a GM of 3dB are then written as

TABLE II
PARAMETERS OF THE CIRCUITS

Symbol	Quantity	Value
V_{dc}	DC input voltage amplitude	450 V
v_g	Single-phase grid voltage amplitude	155 V
L_i	Inverter side inductor	4.4 mH
L_g	Grid side inductor	2.2 mH
C	Capacitor of *LCL* filter	10 μF
ω_r	Resonance angular frequency of L_g and C	6742 rad/s
ω_{res}	Resonance angular frequency	8257.2 rad/s
f_{res}	Resonance frequency	1314.2 Hz
ω_n	Fundamental angular frequency	2π·50 rad/s

$$\begin{cases}k_{p\max}=\dfrac{\omega_s L_i[4(2\lambda+1)^2\omega_{res}^2-\omega_s^2]}{8k_{PWM}(2\lambda+1)^3\omega_r^2},\\ k_{p4}=\dfrac{\sqrt{2}\omega_s L_i[4(2\lambda+1)^2\omega_{res}^2-\omega_s^2]}{16k_{PWM}\omega_r^2(2\lambda+1)^3}.\end{cases} \tag{41}$$

Then k_p is chosen to be the smallest value among k_{p1}, k_{p2}, k_{p3}, and k_{p4}.

Finally, the integral gain k_i is tuned to have a small influence on the phase at ω_{g1}:

$$k_i=\frac{\omega_{g1}}{10}=\frac{\pi-2\varphi}{10(2\lambda+1)T_s}. \tag{42}$$

VI. RESULTS

Simulations and experiments were implemented to verify the delay-dependent stability of the single-loop controlled grid-connected inverters with *LCL* filters. Parameters of the circuits are given in Table II. The control is implemented in the synchronous *dq* frame, thus decoupling terms are used [19]. The transient response as the amplitude of the grid current stepping from 1 A to 4 A is examined to evaluate the system stability. Therefore it is achieved by stepping the reference *d* current from 1 A to 4 A. For GCF, the reference *q* current is set to 0. For ICF, as the grid current is indirectly controlled, the reference *q* current is set to $\omega_n C v_g$ instead of 0 to achieve unity power factor [10].

A. Simulation Results

Simulations in MATLAB/PLECS were used to verify the stable ranges of the time delay obtained in Section II and III. Taking $f_s=6f_{res}$ for example, $\omega_{res}T_s<\pi$ is fulfilled, therefore the stable ranges (6) and (21) of the ICF are identical, as well as the stable ranges (9) and (23) of the GCF.

The reference *d* current steps from 1 A to 4 A at 0.02 s. For ICF, the transient responses when $T_d<\pi/2\omega_{res}(k=0)$, $3\pi/2\omega_{res}<T_d<5\pi/2\omega_{res}(k=1)$, and $7\pi/2\omega_{res}<T_d<9\pi/2\omega_{res}(k=2)$ are shown in Fig. 15, the lags in the responses are due to the time delay in the forward-loop. It can be seen that when the time delay is within these ranges, the ICF loop can be made stable. The instabilities when T_d is outside the stable ranges are also shown in Fig. 15, where the range of T_d changes at 0.08 s. For $k\geq 3$ in (6), although not shown here, the loop can also be made stable. However, as can be seen from Fig. 15, for a larger k, a slower transient response is produced because of the lower bandwidth.

For GCF, the stable transient responses when $\pi/2\omega_{res}<T_d<3\pi/2\omega_{res}(k=0)$, $5\pi/2\omega_{res}<T_d<7\pi/2\omega_{res}(k=1)$, and $9\pi/2\omega_{res}$

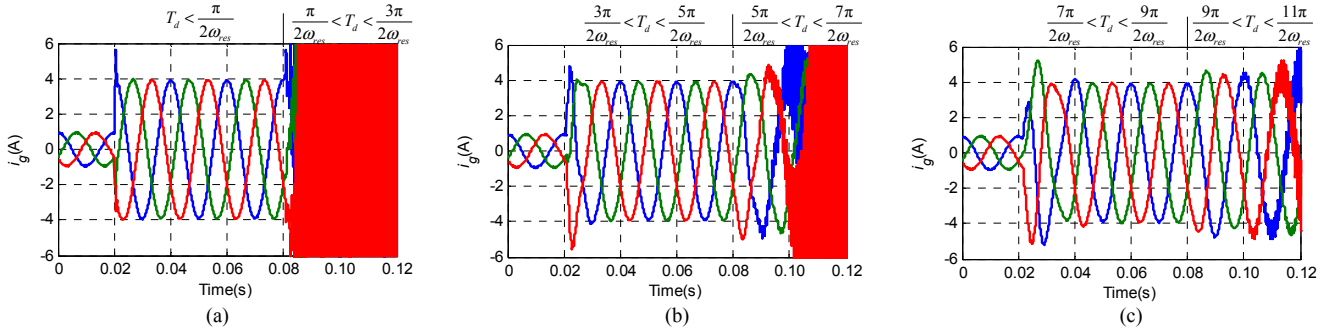

Fig. 15. Simulated transient responses of ICF when T_d is in different ranges. (a) $T_d < \pi/2\omega_{res}$, $\pi/2\omega_{res} < T_d < 3\pi/2\omega_{res}$. (b) $3\pi/2\omega_{res} < T_d < 5\pi/2\omega_{res}$, $5\pi/2\omega_{res} < T_d < 7\pi/2\omega_{res}$ (c) $7\pi/2\omega_{res} < T_d < 9\pi/2\omega_{res}$, $9\pi/2\omega_{res} < T_d < 11\pi/2\omega_{res}$.

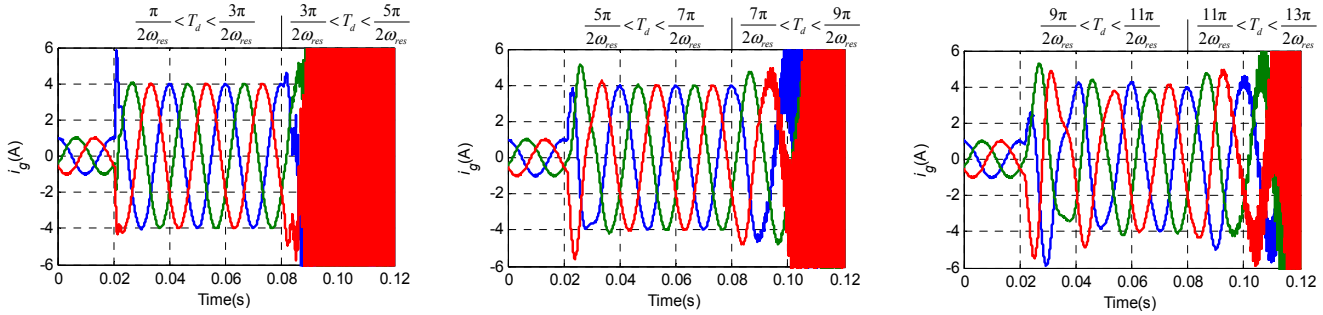

Fig. 16. Simulated transient responses of GCF when T_d is in different ranges. (a) $\pi/2\omega_{res} < T_d < 3\pi/2\omega_{res}$, $3\pi/2\omega_{res} < T_d < 5\pi/2\omega_{res}$. (b) $5\pi/2\omega_{res} < T_d < 7\pi/2\omega_{res}$, $7\pi/2\omega_{res} < T_d < 9\pi/2\omega_{res}$. (c) $9\pi/2\omega_{res} < T_d < 11\pi/2\omega_{res}$, $11\pi/2\omega_{res} < T_d < 13\pi/2\omega_{res}$.

$< T_d < 11\pi/2\omega_{res}$ ($k = 2$) and the unstable responses when T_d is outside the stable ranges are shown in Fig. 16. For $k \geq 3$ in (9), the GCF loop can also be stabilized with well-designed controller parameters. If the time delay is not within the stable ranges, the system can never be stabilized with any controller gain.

These simulated results verify the stable ranges of time delay derived in Section II and III.

B. Experimental Results

Experiments were conducted on a three-phase grid-connected inverter prototype shown in Fig. 17. The prototype comprises a Semikron power processing device (contains a three-phase IGBT inverter), a DSP control board (TMS320F28335), a three-phase *LCL* circuit, several circuit breakers, and an isolated 1:2 step-up transformer connected to the power grid. The prototype has a hardware protection circuit based on Altera PLD MAX 3000A and a complete software protection design. In case that any error signal (IGBT switching fault or TI DSP failure) occurs or an overcurrent is detected, the protection will disable the PWM outputs and trigger the operation of circuit breakers, then the system is disconnected from the power grid and stops working.

Because in the real operation the normal values of λ are 0.5 and 1, experiments are implemented to verify the stable range of f_s in Table I, and to validate the time delay compensators and PI design method. The uniformly sampled symmetric-on-time triangle PWM is applied. Samplings are conducted when the PWM counter reaches the period value. $\lambda = 0.5$ is achieved by updating the duty ratio to the compare register when the counter reaches zero, while $\lambda = 1$ is realized by updating the compare register when the counter reaches the period value [9].

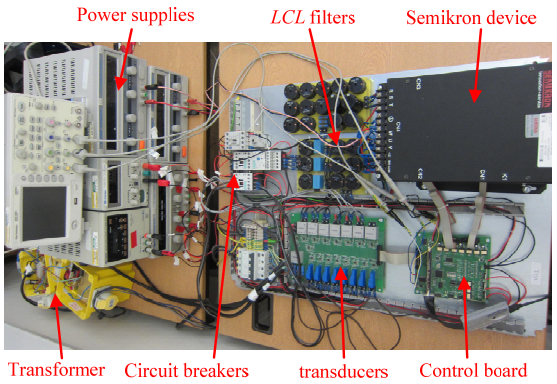

Fig. 17. A three-phase *LCL*-filtered grid-connected inverter system used in the experimental verification of the delay-dependent stability.

The parasitic resistance of the inductors improves system stability, but it does not affect the evaluation of the stable ranges, because if the time delay is outsider the stable ranges the system would be unstable with even a small k_p. For the cases with time delay in the optimal range, controller parameters are designed using the method in Section V. For other cases, comprised parameters are used to validate the stable ranges.

1) Inverter Current Feedback

Fig. 18 shows the one-phase grid voltage and grid current. As can be seen the grid current is synchronized with the grid voltage when it is controlled indirectly by the inverter current.

For $\lambda = 0.5$, as shown in Table I $f_s = 4f_{res}$ is the critical value, below which the system is unable to be stabilized. When $f_s = 6f_{res}$, the transient response is shown in Fig. 19, which indicates the stable operation. When $f_s = 4f_{res}$, the system is marginally stable, as presented in Fig. 20 where the steady-state oscillation

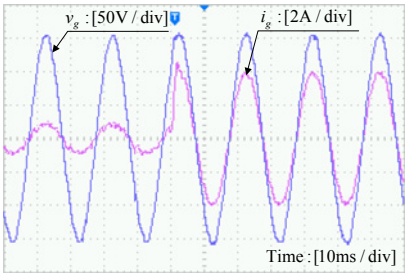

Fig. 18. Experimental single-phase grid voltage and grid current of ICF with $\lambda = 0.5, f_s = 7f_{res}$.

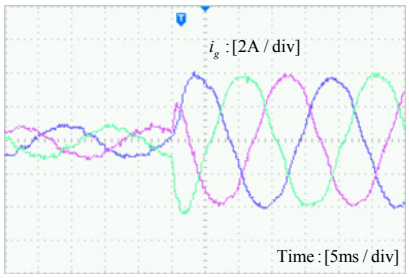

Fig. 19. Experimental transient response of ICF with $\lambda = 0.5, f_s = 6f_{res}$.

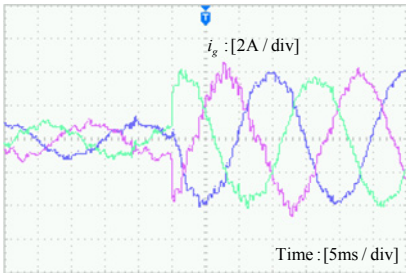

Fig. 20. Experimental transient response of ICF with $\lambda = 0.5, f_s = 4f_{res}$.

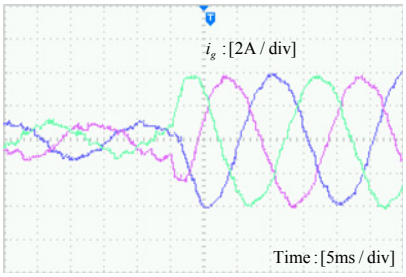

Fig. 21. Experimental transient response of ICF with $\lambda = 0.5, f_s = 4f_{res}$, with linear predictor.

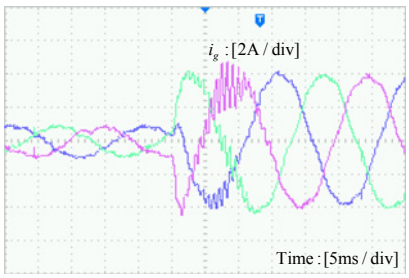

Fig. 22. Experimental transient response of ICF with $\lambda = 1, f_s = 6f_{res}$.

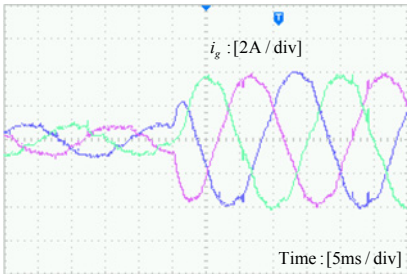

Fig. 23. Experimental transient response of ICF with $\lambda = 1, f_s = 6f_{res}$, with linear predictor.

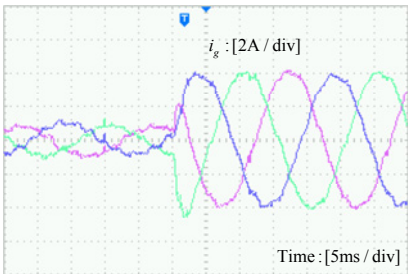

Fig. 24. Experimental transient response of ICF with $\lambda = 1, f_s = 10f_{res}$.

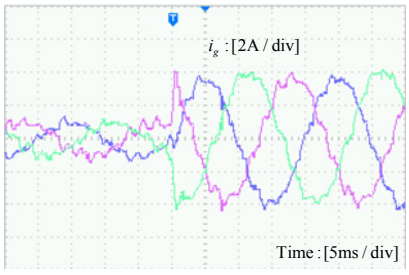

Fig. 25. Experimental transient response of GCF with $\lambda = 0.5, f_s = 4f_{res}$.

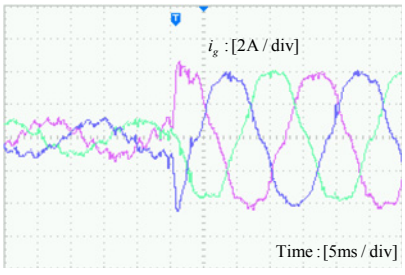

Fig. 26. Experimental transient response of GCF with $\lambda = 0.5, f_s = 6f_{res}$, a delay of $2T_s$ added.

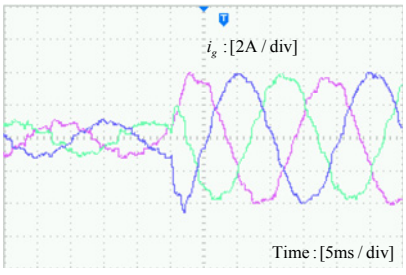

Fig. 27. Experimental transient response of GCF with $\lambda = 1, f_s = 4f_{res}$.

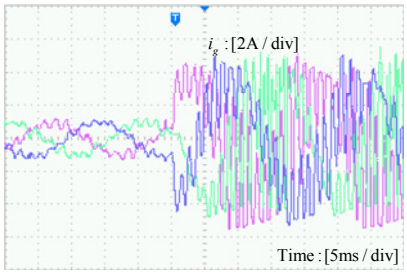

Fig. 28. Experimental transient response of GCF with $\lambda = 1, f_s = 6f_{res}$.

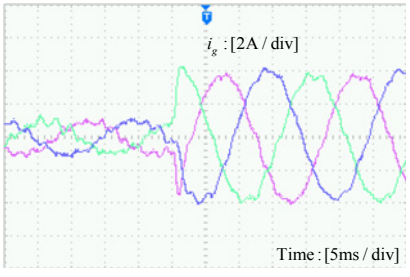

Fig. 29. Experimental transient response of GCF with $\lambda = 1, f_s = 7f_{res}$, a delay of $2T_s$ added.

appears. Although not shown here, when $f_s < 4f_{res}$ the system is more likely to be unstable. However, if a linear predictor is used when $f_s = 4f_{res}$, the transient response is shown in Fig. 21. It can be seen that the linear predictor stabilizes the system, thus the stable range of the sampling frequency is increased.

For $\lambda = 1, f_s > 6f_{res}$ is required for stability. When $f_s = 6f_{res}$, the transient response is shown in Fig. 22, the current ripples imply the weak stability. Compared with the case of $\lambda = 0.5$, the increase in the time delay degrades the stability of the ICF system. However, with the adoption of the linear predictor, the system is stabilized, as shown in Fig. 23. When $f_s = 10f_{res}$, the response in Fig. 24 indicates a stable system.

These experimental results verify the stable ranges of the sampling frequency deduced previously from the stable ranges of time delay. The stability improvement due to the linear predictor has also been verified.

2) Grid Current Feedback

For $\lambda = 0.5$, $2f_{res} < f_s < 4f_{res}$ is required for stability. When $f_s = 4f_{res}$, the transient response shown in Fig. 25 indicates the critical stability. The system is unstable when $f_s > 4f_{res}$ irrespective of the controller parameters. To improve the stability when a high sampling frequency is used, a proper time delay is added. Taking $f_s = 6f_{res}$ for example, by adding a delay of $2T_s$, the system is stabilized, as shown in Fig. 26.

For $\lambda = 1$, $2f_{res} < f_s < 6f_{res}$ is the stable range. When $f_s = 4f_{res}$ the transient response in Fig. 27 shows a stable operation. Compared with that of $\lambda = 0.5$, it is obvious that the time delay improves the stability and increases the stable range of the sampling frequency. The transient response when $f_s = 6f_{res}$ is shown in Fig. 28. In this case the system is obvious unstable, and circuit breaks are opened due to the overcurrent. To enhance the stability, a proper time delay should be added. Taking $f_s = 7f_{res}$ for instance, an additional delay of $2T_s$ is also used. The transient response is given in Fig. 29, which shows the improvement on stability due to the time delay addition.

The above results validate the stable ranges of sampling frequency in Table I which are deduced from the study of time delay requirements. It is also verified that the stability of the GCF system can be enhanced by using the delay addition method when a high sampling frequency is used.

VII. Conclusion

A systematic study of the relationship between the time delay and stability of single-loop controlled grid-connected inverters with *LCL* filters has been carried out. The stable ranges of time delay for the inverter current feedback loop and grid current feedback loop are obtained, in the continuous *s*-domain and also the discrete *z*-domain. The optimal range of the time delay is also discussed. To improve system stability, a linear predictor based time delay reduction method is proposed for the inverter current feedback, whereas a proper time delay is added for the grid current feedback. The available sampling frequency ranges are therefore increased. Furthermore, a simple PI controller design method has been presented, by which adequate stability margins can be guaranteed. Simulation and experimental results have validated the study of the delay-dependent stability. This study has, for the first time, explained why different conclusions on the stability of the single-loop control systems were drawn in different previous studies. Furthermore, the procedure can be extended to analyze the influence of time delay on the stability of *LCL*-filtered grid-connected inverters controlled by other methods including active damping.

Appendix

This is a derivation example of the stable ranges of time delay in the discrete *z*-domain.

For the GCF, $G_g(z)$ in (17) can be written as

$$G_g(z) = \frac{k_{PWM}}{(L_i + L_g)\omega_{res}} \frac{z^3 a + z^2 b + zc + d}{z^{\ell}(z^3 - z^2 e + ze - 1)}, \quad \text{(A.1)}$$

with $a = m\theta - \sin m\theta$, $b = (1-m)\theta - \sin(1-m)\theta + 2\sin m\theta - 2m\theta\cos\theta$, $c = m\theta - 2(1-m)\theta\cos\theta - \sin m\theta + 2\sin(1-m)\theta$, $d = (1-m)\theta - \sin(1-m)\theta$, $e = 2\cos\theta + 1$, and $\theta = \omega_{res}T_s$ ($\theta < \pi$). With $G_c(s) = k_p$, the denominator of the closed-loop transfer function (19) is denoted as

$$D(z) = z^{\ell+3} - z^{\ell+2}e + z^{\ell+1}e - z^{\ell} + z^3 Ka + z^2 Kb + zKc + Kd \quad \text{(A.2)}$$

where $K = \frac{k_p k_{PWM}}{(L_i + L_g)\omega_{res}}$.

Taking $\ell = 1$ and $0 \le m < 1$, i.e., $0 < \lambda$ ($\lambda = \ell - m$) ≤ 1 for example, in this case $D(z) = z^4 + (Ka - e)z^3 + (Kb + e)z^2 + (Kc - 1)z + Kd$. Using the *w*-transform $z = (w+1)/(w-1)$, $D(w)$ can be expressed as

$$D(w) = D(z)\big|_{z=\frac{w+1}{w-1}} = \frac{Aw^4 + Bw^3 + Cw^2 + Dw + E}{(w-1)^4}, \quad \text{(A.3)}$$

with $A = K(a + b + c + d)$, $B = 2(3 + Ka - Kc - 2Kd - e)$, $C = 2(3 - Kb + 3Kd - e)$, $D = 2(1 - Ka + Kc - 2Kd + e)$, $E = 2 - Ka + Kb - Kc + Kd + 2e$. Defining $e_1 = 1 + e = 2(1 + \cos\theta)$, $e_2 = 3 - e = 2(1 - \cos\theta)$, $K_1 = K(a - c - 2d)$, $K_2 = K(-b + 3d)$, $K_3 = K(-a + c - 2d)$, and $K_4 = K(-a + b - c + d)$, we have:

$$\begin{aligned} &A = K\theta e_2, B = 2(e_2 + K_1), C = 2(e_2 + K_2), \\ &D = 2(e_1 + K_3), E = 2e_1 + K_4. \end{aligned} \quad \text{(A.4)}$$

Note that $0 < \theta < \pi$, $e_1 > 0$ and $e_2 > 0$ are obtained, hence $A > 0$, $B > 0$, $C > 0$, $D > 0$, and $E > 0$.

To ensure system stability, all of the roots of the characteristic equation $Aw^4 + Bw^3 + Cw^2 + Dw + E = 0$ should be in the LPH, this can be evaluated using the Routh's stability criterion. The Routh array of $Aw^4 + Bw^3 + Cw^2 + Dw + E = 0$ is given as:

w^4:	A	C	E
w^3:	B	D	
w^2:	$\frac{BC - AD}{B}$	E	
w^1:	$D - \frac{B^2 E}{BC - AD}$		
w^0:	E		

$A > 0$, $B > 0$, and $E > 0$ have been satisfied. To ensure stability $BC - AD > 0$ and $BCD - AD^2 - B^2E > 0$ are also required, i.e.,

$$\begin{cases} 2(e_2 + K_1)(e_2 + K_2) > K\theta e_2(e_1 + K_3) \\ 2(e_2 + K_1)(e_2 + K_2)(e_1 + K_3) > \\ \quad K\theta e_2(e_1 + K_3)^2 + (e_2 + K_1)^2(2e_1 + K_4) \end{cases} \quad \text{(A.5)}$$

Note that K_1, K_2, K_3, and K_4 all contain a factor of K, the first inequality can be fulfilled using an infinitely small K (i.e., by setting an infinitely small k_p). The second inequality can be simplified to (A.6) below when an infinitely small K is used so that the second-order and third-order terms for K can be eliminated.

$$(2K_3 - K_4)e_2 + 2(K_2 - K_1)e_1 > K\theta e_1^2 \quad \text{(A.6)}$$

Eliminating K in (A.6) gives

$$(-a - b + 3c - 5d)(3 - e) + 2(-a - b + c + 5d)(1 + e) > \theta(1 + e)^2, \quad \text{(A.7)}$$

which can be converted to

$$\begin{aligned} &\sin[(2-m)\theta] < \sin[(1-m)\theta] \\ &\Rightarrow \sin[(\lambda+1)\omega_{res}T_s] < \sin(\lambda\omega_{res}T_s). \end{aligned} \quad \text{(A.8)}$$

Finally, because $\omega_{res}T_s < \pi$ and in this GCF example $0 < \lambda \le 1$, the following stable range of time delay is obtained

$$\frac{\pi}{2\omega_{res}} < (\lambda + \frac{1}{2})T_s < (\lambda + \frac{1}{2})\frac{\pi}{\omega_{res}}, (0 < \lambda \le 1). \quad \text{(A.9)}$$

References

[1] M. Liserre, F. Blaabjerg, and S. Hansen, "Design and control of an LCL-filter-based three-phase active rectifier," *IEEE Trans. Ind. Appl.*, vol. 41, no. 5, pp. 1281-1291, Sep./Oct. 2005.

[2] J. Dannehl, C. Wessels, and F. W. Fuchs, "Limitations of voltage-oriented PI current control of grid-connected PWM rectifiers with LCL filters," *IEEE Trans. Ind. Electron.*, vol. 56, no. 2, pp. 380-388, Feb. 2009.

[3] J. He and Y. W. Li, "Generalized closed-loop control schemes with embedded virtual impedances for voltage source converters with LC or

LCL filters," *IEEE Trans. Power Electron.*, vol. 27, no. 4, pp. 1850-1861, Apr. 2012.
[4] L. Harnefors, A. G. Yepes, A. Vidal, and J. Doval-Gandoy, "Passivity-based stabilization of resonant current controllers with consideration of time delay," *IEEE Trans. Power Electron.*, vol. 29, no. 12, pp. 6260-6263, Dec. 2014.
[5] R. Pena-Alzola, M. Liserre, F. Blaabjerg, R. Sebastián, J. Dannehl, and F. W. Fuchs, "Analysis of the Passive Damping Losses in LCL-filter Based Grid Converters," *IEEE Trans. Power Electron.*, vol. 28, no. 6, pp. 2642-2646, Jun. 2013.
[6] C. Bao, X. Ruan, X. Wang, W. Li, D. Pan, and K. Weng, "Step-by-step controller design for LCL-Type Grid-Connected inverter with capacitor-current-feedback active-damping," *IEEE Trans. Power Electron.,* vol. 29, no. 3, pp. 1239-1253, Mar. 2014.
[7] F. Liu, Y. Zhou, S. Duan, J. Yin, B. Liu, and F. Liu, "Parameter design of a two-current-loop controller used in a grid-connected inverter system with LCL filter," *IEEE Trans. Ind. Electron.*, vol. 56, no. 11, pp. 4483-4491, Nov. 2009.
[8] J. Dannehl, M. Liserre, and F. W. Fuchs, "Filter-based active damping of voltage source converters with LCL filter," *IEEE Trans. Ind. Electron.,* vol. 58, no. 8, pp. 3623-3633, Aug. 2011.
[9] X. Zhang, J. W. Spencer, and J. M. Guerrero, "Small-signal modeling of digitally controlled grid-connected inverters with LCL filters," *IEEE Trans. Ind. Electron.*, vol. 60, no. 9, pp. 3752-3765, Sep. 2013.
[10] Y. Tang, P. C. Loh, P. Wang, F. H. Choo, and F. Gao, "Exploring inherent damping characteristic of LCL-filters for three-phase grid-connected voltage source inverters," *IEEE Trans. Power Electron.*, vol. 27, no. 3, pp. 1433-1443, Mar. 2012.
[11] M. Liserre, R. Teodorescu, and F. Blaabjerg, "Stability of photovoltaic and wind turbine grid-connected inverters for a large set of grid impedance values," *IEEE Trans. Power Electron.*, vol. 21, no. 1, pp. 263-272, Jan. 2006.
[12] M. Castilla, J. Miret, A. Camacho, J. Matas, and L. G. de Vicuna, "Reduction of Current Harmonic Distortion in Three-Phase Grid-Connected Photovoltaic Inverters via Resonant Current Control," *IEEE Trans. Ind. Electron.*, vol. 60, no. 4, pp. 1464-1472, Apr. 2013.
[13] A. Kahrobaeian and Y. Ibrahim, "Robust Single-Loop Direct Current Control of LCL-Filtered Converter-based DG Units in Grid-Connected and Autonomous Microgrid Modes," *IEEE Trans. Power Electron.,* vol. 29, no. 10, pp. 5605-5619, Oct. 2014.
[14] R. Teodorescu, F. Blaabjerg, M. Liserre, and A. Dell'Aquila, "A stable three-phase LCL-filter based active rectifier without damping," in *Proc. 2003 IEEE Ind. Appl. Soc. Annu. Meeting*, pp. 1552-1557.
[15] J. Yin, S. Duan, and B. Liu, "Stability Analysis of Grid-Connected Inverter with LCL Filter Adopting A Digital Single-Loop Controller with Inherent Damping Characteristic," *IEEE Trans. Ind. Inform*., vol. 9, no. 2, pp. 1104-1112, May. 2013.
[16] S. G. Parker, B. P. McGrath, and D. G. Holmes, "Regions of Active Damping Control for LCL Filters," *IEEE Trans. Ind. Appl.*, vol. 50, pp. 424-432, Jan/Feb. 2014.
[17] R. Li, B. Liu, S. Duan, J. Yin, and X. Jiang, "Analysis of delay effects in single-loop controlled grid-connected inverter with LCL filter," in *Proc. IEEE Appl. Power Elec. Conf*., 2013, pp. 329-333.
[18] C. Zou, B. Liu, S. Duan, and R. Li, "Influence of Delay on System Stability and Delay Optimization of Grid-Connected Inverters With LCL Filter," *IEEE Trans. Ind. Inform*., vol. 10, no. 3, pp. 1775-1784, Aug. 2014.
[19] J. Dannehl, F. W. Fuchs, and P. B. Thøgersen, "PI state space current control of grid-connected PWM converters with LCL filters," *IEEE Trans. Power Electron.,* vol. 25, no. 9, pp. 2320-2330, Sep. 2010.
[20] Y. Ren and J. Fang, "Current-Sensing Resistor Design to Include Current Derivative in PWM H-Bridge Unipolar Switching Power Amplifiers for Magnetic Bearings," *IEEE Trans. Ind. Electron.,* vol. 59, no. 12, pp. 4590-4600, Nov. 2012.
[21] J. Xu, S. Xie, and T. Tang, "Active Damping-Based Control for Grid-Connected LCL-Filtered Inverter With Injected Grid Current Feedback Only," *IEEE Trans. Ind. Electron.*, vol. 61, no. 9, pp. 4746-4758, Sep. 2014.
[22] E. Twining and D. G. Holmes, "Grid current regulation of a three-phase voltage source inverter with an LCL input filter," *IEEE Trans. Power Electron.*, vol. 18, no. 3, pp. 888-895, May 2003.
[23] M. H. Bierhoff and F. W. Fuchs, "Active damping for three-phase PWM rectifiers with high-order line-side filters," *IEEE Trans. Ind. Electron.*, vol. 56, no. 2, pp. 371-379, Feb. 2009.
[24] V. Miskovic, V. Blasko, T. Jahns, A. Smith, and C. Romenesko, "Observer based active damping of LCL resonance in grid connected voltage source converters," *IEEE Trans. Ind. Appl.*, vol. 50, no. 6, pp. 3977-3985, Nov/Dec 2014.
[25] X. Wang, F. Blaabjerg, and P. Loh, "Virtual RC Damping of LCL-Filtered Voltage Source Converters with Extended Selective Harmonic Compensation." *IEEE Trans. Power Electron.,* to be published.
[26] J. Dannehl, F. W. Fuchs, S. Hansen, and P. B. Thøgersen, "Investigation of active damping approaches for PI-based current control of grid-connected pulse width modulation converters with LCL filters," *IEEE Trans. Ind. Appl*., vol. 46, no. 4, pp. 1509-1517, Jul./Aug. 2010.
[27] S. Bibian and H. Jin, "Time delay compensation of digital control for DC switchmode power supplies using prediction techniques," *IEEE Trans. Power Electron.,* vol. 15, no. 5, pp. 835-842, Sep. 2000.
[28] T. Nussbaumer, M. L. Heidwein, G. Gong, S. D. Round, and J. W. Kolar, "Comparison of Prediction Techniques to Compensate Time Delays Caused by Digital Control of a Three-Phase Buck-Type PWM Rectifier System," *IEEE Trans. Ind. Electron.*, vol. 55, no. 2, pp. 791-799, Feb. 2008.
[29] D. G. Holmes, T. A. Lipo, B. P. McGrath, and W. Y. Kong, "Optimized design of stationary frame three phase AC Current regulators," *IEEE Trans. Power Electron.*, vol. 24, no. 11, pp. 2417-2426, Nov. 2009.
[30] D. M. Van de Sype, K. De Gussemé, F. M. L. L. De Belie, A. P. Van den Bossche, and J. A. Melkebeek, "Small-signal z-domain analysis of digitally controlled converters," *IEEE Trans. Power Electron*., vol. 21, no. 2, pp. 470-478, Mar. 2006.
[31] X. Zhang and J. W. Spencer, "Study of multisampled multilevel inverters to improve control performance," *IEEE Trans. Power Electron*., vol. 27, no. 11, pp. 4409-4416, Nov. 2012.
[32] D. Pan, X. Ruan, C. Bao, W. Li, and X. Wang, "Capacitor-Current-Feedback Active Damping With Reduced Computation Delay for Improving Robustness of LCL-Type Grid-Connected Inverter," *IEEE Trans. Power Electron.*, vol. 29, no. 7, pp. 3414-3427, Jul. 2014.
[33] P. Mattavelli, F. Polo, F. Dal Lago, and S. Saggini, "Analysis of control-delay reduction for the improvement of UPS voltage-loop bandwidth," *IEEE Trans. Ind. Electron.*, vol. 55, no. 8, pp. 2903-2911, Aug. 2008.
[34] I. J. Gabe, V. F. Montagner, and H. Pinheiro, "Design and implementation of a robust current controller for VSI connected to the grid through an LCL filter," *IEEE Trans. Power Electron*., vol. 24, no. 6, pp. 1444-1452, Jun. 2009.
[35] M. Castilla, J. Miret, J. Matas, L. G. de Vicuña, and J. M. Guerrero, "Control design guidelines for single-phase grid-connected photovoltaic inverters with damped resonant harmonic compensators," *IEEE Trans. Ind. Electron.*, vol. 56, no. 11, pp. 4492-4501, Nov. 2009.

Jianguo Wang (S'14) was born in Jiangxi Province, China, in 1988. He received the B.S. and M.S. degrees in electrical engineering from Dalian University of Technology, Dalian, China, in 2010 and 2013, respectively.

Since 2012, he has been with the Department of Electrical Engineering and Electronics, University of Liverpool, UK. His research interests include the control of power electronics and renewable energy generation system.

Jiu Dun Yan (M'03) received the BEng and MEng degrees from the Department of Engineering Mechanics, Tsinghua University, Beijing, China, in 1986 and 1988, respectively. He then worked in Xi'an High Voltage Research Institute (now XIHARI) in China for 6 years, engaged in the R&D of high voltage switchgear, before he joined the University of Liverpool where he studied for and was awarded in 1998 his PhD degree.

He is currently a Reader at the University of Liverpool with research interests in switching arcs and its numerical modelling, thermal management for high voltage equipment, intelligent circuit breakers, electric discharges under HVDC stress and power electronics based inverter systems for grid connection of renewable power generation systems. He has published a total of 115 refereed journal and conference papers.

Lin Jiang (M'00) received the B.Sc. and M.Sc. degrees from Huazhong University of Science and Technology, Wuhan, China, in 1992 and 1996, respectively, and the Ph.D. degree from The University of Liverpool, Liverpool, U.K., in 2001, all in electrical engineering.

He was a Postdoctoral Research Assistant with The University of Liverpool, Liverpool, U.K., from 2001 to 2003 and a Postdoctoral Research Associate with the Department of Automatic Control and Systems Engineering, University of Sheffield, Sheffield, U.K., from 2003 to 2005. He was a Senior Lecturer with the University of Glamorgan from 2005 to 2007 and joined the University of Liverpool in 2007. Currently, he is a Senior Lecturer with The University of Liverpool. His current research interests include control and analysis of power system, smart grid, and renewable energy.

Jiyan Zou received the B.S. degree from the Department of electrical engineering, Shenyang University of Technology, M.S. degree from Institute of Electrical Engineering(IEE) of Sino-Academy, and PhD degree in electrical engineering from Xi'an Jiaotong University, Xi'an, China.

He was a research associate in IEE of Sino-Academy from 1982 to 1984, before with Huazhong University of Science and Technology from 1990 to 1998. He is a Member of Council of Sino-Electric Engineering Institute (CIEE), and the Vice-chairmen of Arcs and Electric Contact Committee and Electromagnetic Launch Committee of CIEE. Since 1999, as a Professor he has been with the School of Electrical Engineering, Dalian University of Technology, Dalian, China. His research interests include research and applications on intelligent power apparatus, intelligent detection and state monitoring technology, high voltage engineering and pulse power technology, theory and applications on arcs and electric contacts, and power electronics.